Heliyon 10 (2024) e32474

Contents lists available at ScienceDirect

Heliyon

journal homepage: www.cell.com/heliyon

Research article

The combined use of serum Raman spectroscopy and D dimer testing for the early diagnosis of acute aortic dissection

Xuechang Han [a,b,1], Shuang Wang [c,1], Runlu Cai [a], Qiang Chen [d], Jing Li [d], Liang Zhong [d], Shuman Ji [a], Xiaopeng Mei [a], Rongqian Wu [e], Yang Yan [d,***], Yi Lv [e,**], Zhanqin Zhang [a,*]

[a] Department of Anesthesiology, The First Affiliated Hospital of Xi'an Jiaotong University, Xi'an, China
[b] Department of Anesthesiology, The First Affiliated Hospital and College of Clinical Medicine of Henan University of Science and Technology, Luoyang, China
[c] Institute of Photonics and Photon-Technology, Northwest University, Xi'an, China
[d] Department of Cardiovascular Surgery, The First Affiliated Hospital of Xi'an Jiaotong University, Xi'an, China
[e] National Local Joint Engineering Research Center for Precision Surgery & Regenerative Medicine, Shaanxi Provincial Center for Regenerative Medicine and Surgical Engineering, The First Affiliated Hospital of Xi'an Jiaotong University, Xi'an, China

ARTICLE INFO

Keywords:
Optical diagnostics
Raman spectroscopy
Acute aortic dissection
Early detection
D-dimer

ABSTRACT

Objectives: Acute aortic dissection (AAD) is an extremely life-threatening medical emergency, often misdiagnosed in its early stages, resulting in prolonged wait times for rescue. This study aims to identify potential serum biomarkers that can assist in the accurate diagnosis of AAD and effectively differentiate it from other conditions causing severe chest pain.

Methods: A total of 122 patients with AAD and 129 patients with other severe chest pain disorders were included in the study. Serum samples were analyzed by measuring the peak intensities of Raman spectra. For each measurement, the Raman spectrum was accumulated by two accumulations (3 s per acquisition). Logistic regression and nomogram models were developed using these peak intensities as well as D-dimer levels to predict the occurrence of AAD. The clinical utilities of these models were assessed through receiver operating characteristics (ROC) curve analysis, net reclassification improvement (NRI), integrated discrimination improvement (IDI), and decision curve analysis (DCA) in both training and internal test cohorts.

Results: The D-dimer levels of AAD patients were significantly increased, as well as higher intensities at specific Raman peaks, including 505 cm^{-1}, 842 cm^{-1}, 947 cm^{-1}, 1254 cm^{-1}, 1448 cm^{-1}, and 1655 cm^{-1} when compared to non-AAD patients. Conversely, decreased intensities were observed at Raman peaks such as 750 cm^{-1}, 1004 cm^{-1}, 1153 cm^{-1}, 1208 cm^{-1}, and 1514 cm^{-1} in AAD patients. Least absolute shrinkage and selection operator regression analysis on the training cohort identified eight potential predictors: D-dimer along with intensity measurements at peaks such as 505 cm^{-1}, 750 cm^{-1}, 1153 cm^{-1}, 1208 cm^{-1}, 1254 cm^{-1}, 1448 cm^{-1}, and 1655 cm^{-1}. The combination of these eight potential predictors demonstrated a good discriminatory performance, with an area under the curve (AUC) value of 0.928 in the training cohort and an AUC of 0.936 in the internal test cohort, outperforming the use of D-dimer alone. Furthermore,

* Corresponding author.
** Corresponding author.
*** Corresponding author.
E-mail addresses: yangyan3@xjtu.edu.cn (Y. Yan), luyi169@126.com (Y. Lv), zhangzhanqin12@sina.com (Z. Zhang).
[1] These authors contributed equally to this work.

https://doi.org/10.1016/j.heliyon.2024.e32474
Received 9 January 2024; Received in revised form 29 May 2024; Accepted 4 June 2024
Available online 5 June 2024

DCA curve analysis revealed that leveraging this combination of eight potential predictors would provide substantial net benefits for clinical application. Moreover, this combination significantly augmented discrimination power, as evidenced by a continuous NRI of 39.8 % and IDI of 9.95 % in the training cohort, as well as a continuous NRI of 27.1 % and IDI of 9.95 % in the internal test cohort.

Conclusions: The employment of this combination of eight potential predictors effectively rules out AAD to a greater extent. This study presents a promising diagnostic strategy for early detection using optical diagnostic techniques such as Raman spectroscopy.

1. Introduction

Acute aortic dissection (AAD) is a life-threatening cardiovascular condition that typically occurs within two weeks and progresses rapidly, often leading to vessel rupture, hemorrhage, and even death. Additionally, it can cause ischemic necrosis of vital organs due to the occlusion of crucial distal branch vessels [1]. Symptomatic AAD of the ascending aorta is particularly lethal, with an early mortality rate of 1 %–2 % per hour if left untreated [2]. Patients with uncomplicated acute type B aortic coarctation also exhibit a 30-day mortality rate of 10 % [2]. Consequently, early diagnosis and appropriate intervention are crucial for saving lives. The clinical presentation of AAD is often misdiagnosed, resulting in an overall misdiagnosis rate of 33.8 % in previous studies [3]. AAD is also among the four differential diagnoses of acute chest pain in the emergency department. Distinguishing AAD from other conditions such as acute myocardial infarction (AMI) and pulmonary embolism (PE) poses a significant challenge in achieving rapid and accurate diagnosis. These emergencies share similar clinical features but require different treatment and management strategies. For instance, AMI and PE often require thrombolytic drugs; therefore, misdiagnosing AAD as AMI or PE could result in catastrophic bleeding or worsenAAD [4].

The electrocardiograms and chest radiographs diagnostic accuracy for AAD is presently limited by their insufficient sensitivity and specificity. Conversely, advanced imaging modalities such as computed tomography (CT) and magnetic resonance imaging (MRI) are highly accurate and are considered the preferred diagnostic techniques for AAD [1]. However, their immediate implementation in emergency departments might be constrained. Serologic biomarkers present a convenient, noninvasive, and radiation-free alternative for early diagnosis of AAD. By employing rational biomarkers for initial confirmation, followed by further imaging techniques for accurate diagnosis, the time delay in diagnosing AAD can be significantly reduced. Several biomarkers associated with inflammatory responses and thrombotic processes have been identified, which can indicate early pathophysiological changes in the aortic wall [5]. Presently, D-dimer is the lone clinically relevant biomarker for suspected AAD [5]; nevertheless, its specificity is low in patients with false lumen embolization or less extensive lesions or younger age groups [6]. Although elevated D-dimer levels have been observed in AAD compared to AMI cases, it cannot differentiate between PE and AAD patients [6]. Consequently, identification of additional biomarkers that could provide supplementary information at onset along with D-dimer testing would enhance the early diagnosis reliability of AAD without increasing false positives or negatives.

Raman spectroscopy is a widely used optical analytical technique that allows for the examination of molecular structure and chemical composition in various substances. Its application in the biomedical field has been extensive due to its ability to rapidly analyze samples containing water and its insensitivity to water interference [7]. This technique has demonstrated promising potential for label-free monitoring and clinical diagnosis of various diseases, including cardiovascular disease [8]. Additionally, compared to traumatic tissue sample collection, serum samples offer a less invasive and more cost-effective alternative. Reena V John et al. successfully used Raman spectroscopy on blood samples to investigate inflammation in patients with AMI, achieving an impressive overall accuracy rate of 100 % for distinguishing cases of AMI [9]. Furthermore, our recent study confirmed significant differences in serum Raman spectra between normal individuals and those with cardiac myxoma. This study also identified unique Raman spectral characteristics specific to cardiac myxoma patients for early disease identification [10]. During the formation of AAD, altered metabolites of biomolecules can be detected within the bloodstream circulation [11], indicating the potential of this technology for facilitating early AAD diagnosis.

Logistic regression analysis is frequently used in clinical studies to identify independent factors that can predict a specific outcome. It is a statistical method that allows for estimating the likelihood of an event occurring based on a set of variables [12]. In the context of predicting AAD, logistic regression can help determine which factors significantly contribute to the probability of developing AAD. Furthermore, nomograms have become increasingly popular in clinical prediction modeling due to their ability to visually represent prediction models. Nomograms are graphical tools that enable calculation of an individual's probability of experiencing a particular outcome based on their unique characteristics. They can assist in making clinical decisions by providing an easy-to-use and intuitive approach to assessing risk [12]. The objective of this study is to examine the predictive factors associated with AAD occurrence and create a prediction model using logistic regression analysis and nomograms. By identifying significant predictors and establishing a reliable prediction model, our aim is to enhance early detection of AAD and facilitate timely intervention, ultimately leading to improved patients' outcomes.

2. Materials and methods

2.1. Study population

Consecutive individuals suspected of having AAD and seeking medical attention at the First Affiliated Hospital of Xi'an Jiaotong University from July 2021 to March 2023 were included in this analysis. Patients who met the following compliance criteria [13] were considered eligible for participation in the study: (i) Displaying clinical symptoms suggestive of AAD, such as chest pain, abdominal pain, back pain, syncope, or signs of inadequate blood supply according to the guidelines provided by the American Heart Association in 2010; (ii) Individuals exhibiting no apparent clinical signs or symptoms related to AAD but requiring further imaging tests due to uncertain findings observed during biochemical assessments aimed at confirming or ruling out an AAD diagnosis; (iii) Obtaining informed consent from all participants. Patients meeting any of the following exclusion criteria were excluded: (i) Patients and/or their family members declining diagnostic tests necessary for a definitive diagnosis; (ii) Presence of other conditions such as malignant tumors or hematological disorders; and (iii) Insufficient availability of data.

According to the current guidelines, Aortic Dissection (AD) that occurs within two weeks of symptom onset is referred to as AAD. In contrast, cases presenting after two weeks are categorized as subacute (15–90 days) or chronic AD (>90 days). The Stanford system further classifies AAD into type A and type B. The final diagnosis was made by clinicians not involved in this study based on typical signs or symptoms, chest radiographs, coronary angiograms, echocardiograms, or computed tomography angiograms (CTA). Clinical data were extracted from medical records, while laboratory data were obtained from the hospital's laboratory information system, respectively. This study was approved by the Ethics Review Committee of First Affiliated Hospital of Xi'an Jiaotong University and adhered to the Declaration of Helsinki (revised 2013). Each participant was informed of the purpose of the study and signed a written informed consent form and registered with the ClinicalTrials.gov registry (No. NCT05206032).

2.2. Optical analysis

Sample preparation. The serum samples of all participants were collected from the First Affiliated Hospital of Xi'an Jiaotong University, excluding those required for medical purposes, and were subsequently stored at −80 °C until their utilization. Raman measurement was conducted on air-dried serum samples to improve signal acquisition while ensuring that the droplets formed a coffee-ring shape around the edges. To avoid any chemical or physical inconsistencies after Raman scattering, four to six spectra were obtained from each different serum sample in the center of the coffee ring during regular sampling. In order to prevent interference with glass Raman spectral bands, 1 μL of serum sample was placed onto planar gold-foiled glass slides (pGOLD Slides, Nirmidas Biotech, USA) specifically designed for Raman measurements and allowed to dry for 10 min at a temperature of 18 °C.

Spectral acquisition. The serum samples were analyzed utilizing a confocal Raman spectroscopy system (Alpha 500 R, WITec GmbH, Germany). Prior to the experiment, the spectral wave number was calibrated utilizing an in silico Raman peak at 520.7 cm^{-1}. Subsequently, the experimental parameters were set accordingly. The samples were meticulously positioned on a multi-axis piezo-electric scanning stage, and their precise locations were determined employing a 20 × objective lens (NA = 1, Zeiss, Germany). A semiconductor laser emitting light at an excitation wavelength of 532 nm and a power of 10 mW was utilized to capture the spectral signals from the serum. Each spectrum was acquired with two accumulations and acquisition time of 3 s,. The obtained Raman spectra then underwent preprocessing using WITec Suite FIVE software (WITec GmbH, Germany). Subsequently, normalization of the area under the curve(AUC) within the range of 400∼1800 cm^{-1} was performed utilizing Matlab software (MathWorks, USA) in conjunction with the NWUSA toolbox.

2.3. Statistical analysis

Normality of continuous variables was assessed by the Kolmogorov-Smirnov test. Continuous variables with a normal distribution were presented as mean (standard deviation [SD]); Non-normal data were presented as median (interquartile ranges). Categorical variables were analyzed using chi-square test or Fisher's exact test in the univariate analysis, while continuous variables were examined using Student's t-test or rank-sum test. Spearman correlation analysis was used to evaluate the correlation between the D-dimer levels and the candidated Raman peak intensities. The dataset was randomly divided into training and internal validation cohorts with a ratio of 7:3. We trained and optimized models using the training cohort and validation them on the internal validation cohort.In the training group, multivariate analysis was conducted using Least absolute shrinkage and selection operator (LASSO) logistic regression to identify independent risk factors and develop a predictive nomogram. The performance of the predictive nomogram was evaluated through receiver operating characteristic (ROC) curve and calibration curve analyses, with the area under the ROC curve (AUC) ranging from 0.5 (indicating no discrimination) to 1 (indicating complete discrimination). Additionally, net reclassification improvement (NRI) and integrated discrimination improvement (IDI) were used to give a comprehensive perspective on the predictive performance improves. Decision curve analysis (DCA) was performed to determine the net benefit threshold for prediction. To facilitate integration into clinical practice, an interactive web-based dynamic nomogram application was created using Shiny. In order to facilitate users' operation, the normalized spectral intensities were taken a fourth square root, and the D-dimer value was automatically divided by 100, so that x-axis ranges are unified in the range (0,1). Results with a p-value less than 0.05 were considered statistically significant. All statistical analyses were carried out using R software version 4.2.2 along with MSTATA software (https://www.mstata.com/) for certain procedures.

3. Results

3.1. Patient characteristics

A total of 251 individuals with suspected AAD were included in the study. The primary complaints reported by these individuals were chest pain (61.4 %), back pain (23.1 %), abdominal pain (2.4 %), syncope (4.4 %), and other symptoms (27.1 %), which was consistent with previous findings [14]. Among this group, a diagnosis of AAD was ultimately confirmed in 122 patients (48.6 %), including 80 cases classified as Stanford type A and 42 cases classified as Stanford type B AAD. Initially, AAD was suspected in 129 patients (51.4 %), but later ruled out through CT scanning. The final diagnoses for these patients encompassed acute coronary syndrome (n = 75), acute PE (n = 13), aortic aneurysm without dissection signs(n = 12), inflammatory disease(n = 3) and other conditions(n = 26). Fig. 1 illustrated the patient registration process using a flow chart format. The analysis considered various variables such as gender, age, pain levels, systolic blood pressure(SBP), diastolic blood pressure(DBP), history of hypertension, diabete, smoking habit, and alcohol consumption pattern. In terms of gender distribution between the non-AAD and AAD groups, no significant difference was observed(p value = 0.78). However, the median age among patients diagnosed with AAD was significantly lower than that among non-AAD patients(p value < 0.001). Furthermore, AAD patients exhibited a higher prevalence of pain during hospital visits compared to non-AAD individuals(p value < 0.001). No significant differences were found regarding SBP, DBP, hypertension history, smoking habits, and alcohol consumption between the two groups(p value > 0.05). Nevertheless, the proportion of diabetic individuals within the AAD group exceeded that within the non-AAD group(p value < 0.001).Table 1 displayed the demographic and clinical characteristics for all participants enrolled.

This study evaluated and compared the concentrations of creatinine, lactate dehydrogenase(LDH), troponin-T, brain natriuretic peptide (BNP), and D-dimer in two groups: non-AAD (n = 129) and AAD (n = 122). A significant elevation of D-dimer level was observed in the AAD group (median: 7.45 mg/L, interquartile range [IQR]: 2.32–17.58), in comparison to the non-AAD group (median: 0.39 mg/L, IQR: 0.23–0.76) (p < 0.001), which was consistent with previous findings [14–16]. The median creatinine level in the non-AAD group was recorded at 69 μmol/L (IQR: 58–79), while it was measured at 71 mg/dl (IQR:55–97) in the AAD group; however, no statistically significant difference was detected between these two groups(p = 0.237). Similarly, no significant disparities were observed in LDH(p = 0.427), troponin-T(p = 0.274), and BNP(p = 0.735) levels between both groups.Table 1 displayed the routine biochemical profile of patients diagnosed with AAD and those who received an alternative final diagnosis.

3.2. Raman spectral analysis of serum

The Raman spectra of AAD and non-AAD samples displayed significant disparities in the intensities of spectral bands, which could be attributed to variations in the biological composition of the serum. Averaged and difference Raman spectra were generated for serum samples collected from suspected AAD patients (Fig. 2A and B). To determine whether a statistical distinction exists between the difference spectra of the AAD and non-AAD groups at specific Raman peaks (505 cm^{-1}, 750 cm^{-1}, 842 cm^{-1}, 947 cm^{-1}, 1004 cm^{-1}, 1153 cm^{-1}, 1208 cm^{-1}, 1254 cm^{-1}, 1338 cm^{-1}, 1448 cm^{-1}, 1514 cm^{-1}, and 1655 cm^{-1}), a t-test was performed on two independent samples utilizing spectral intensities as continuous variables(Fig. 2C). Fig. 2A revealed two distinct high-intensity Raman peaks at 1153 cm^{-1} and 1514 cm^{-1}. Due to excitation at 532 nm, the resonance Raman effects were significantly enhanced on these two peaks, which were associated with β-carotene [17]. The intensity levels of these two peaks were lower in serum of AAD patients when compared with non-AAD patients. Furthermore, the intensities of Raman signals corresponding to essential amino acids, such as L-Tryptophan at 750 cm^{-1}, L-Tryptophan at 1208 cm^{-1}, and phenylalanine at 1004 cm^{-1}, were decreased in serum of AAD patients. Compared to the non-AAD group, patients with AAD exhibited higher Raman band intensities at 505 cm^{-1} (L-arginine), 947 cm^{-1}

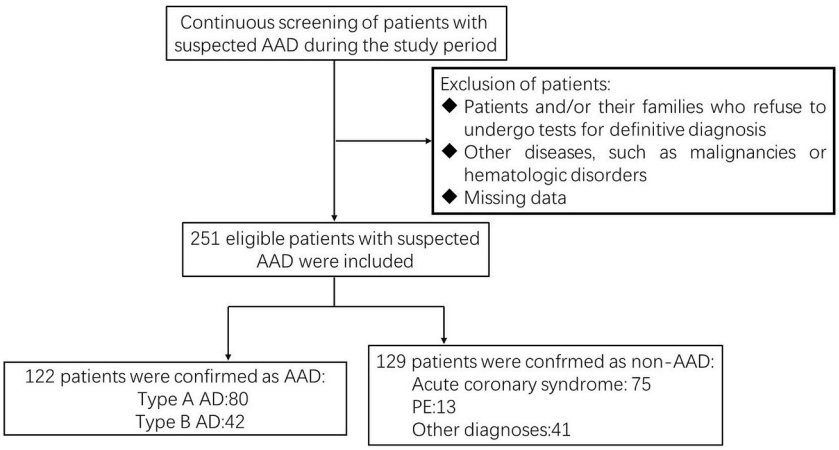

Fig. 1. The flow chart of patient enrollment. AAD, acute aortic dissection; PE, pulmonary embolism.

Table 1
Characteristics and routine biochemical profile of enrolled patients.

Characteristic	groups		*p* value
	Non-AAD, N = 129	AAD, N = 122	
Gender [men,n(%)]			0.78
male	90(69.8 %)	87 (71.3 %)	
female	39 (30.2 %)	35 (28.7 %)	
Age (years)	64 (56, 70)	53 (47, 60)	<0.001
Pain [yes,n(%)]	71 (58.2 %)	114 (88.4 %)	<0.001
SBP	132 ± 22	136 ± 29	0.17
DBP	76 (68, 84)	76 (65, 87)	0.67
Hypertension history [yes,n(%)]	67 (54.9 %)	73 (56.6 %)	0.90
Diabetes history [yes,n(%)]	35 (28.7 %)	6 (4.7 %)	<0.001
Smoking history [yes,n(%)]	59 (48.4 %)	54 (41.9 %)	0.30
Drinking history [yes,n(%)]	28 (23.0 %)	28 (21.7 %)	0.76
Creatinine (umol/L)	69 (58, 79)	71 (55, 97)	0.237
LDH (U/L)	195 (168, 259)	201 (165, 294)	0.427
Troponin-T (ng/ml)	0.011 (0.010, 0.096)	0.012 (0.010, 0.094)	0.274
BNP(pg/ml)	530 (180, 1815)	572 (228, 1345)	0.735
D-dimer (mg/L)	0.39 (0.23, 0.76)	7.45 (2.32, 17.58)	<0.001

SBP is reported as mean ± standard deviation. Age, DBP, Creatinine, LDH, Troponin-T, BNP and D-dimer are reported as Median (IQR). N represents the sample number for each biochemical value. *P* values are calculated with Fisher's exact test or nonparametric Mann-Whitney *U* test. AAD, acute aortic dissection. IQR = interquartile range. LDH = lactate dehydrogenase; BNP = brain natriuretic peptide.

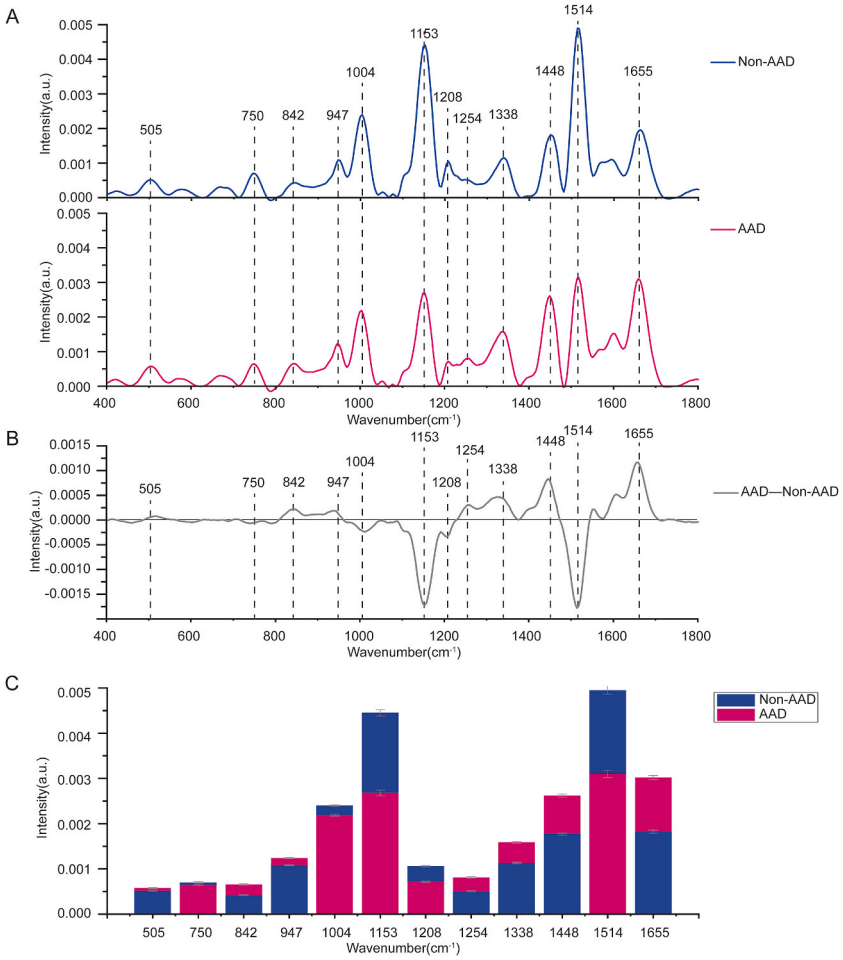

Fig. 2. Comparative analysis of Raman spectral intensities between AAD and non-AAD groups. (A) Representative average Raman spectra for patients with AAD and non-AAD conditions; (B) Spectral pattern differences between the two groups, derived from their respective mean spectra; (C) Intensity variations of specific Raman peaks in AAD and non-AAD groups.

(α-Helix, proline, valine), 1254 cm^{-1} (Amide-III), and 1655 cm^{-1} (α-Helix, Collagen) in their serum. Additionally, an increase in the Raman peak at 1338 cm^{-1} (adenine and guanine) corresponding to DNA base pairs was observed in AAD samples. Furthermore, there was an elevation in the Raman intensity of the peaks at 842 cm^{-1} and 1448 cm^{-1}, which correspond to the CH2 bending mode of phospholipids in AAD samples. Notably, despite similar clinical symptoms between patients with AAD and those with other acute severe chest pain conditions, a significant difference in the mean spectrum of serum between these two groups remained. To gain further insights into the molecular basis underlying these observed Raman spectra of serum samples, Table 2 provided information on variations in the distribution of Raman peaks found in previous literature [18–21].

3.3. Correlation of each different Raman peak intensity of serum with D-dimer

Correlations of each spectral intensity of difference Raman peaks and D-Dimer were shown for both(Fig. 3A), Non-AAD(Fig. 3B) and AAD(Fig. 3C) patients, respectively, with red representing a positive correlation and blue a negative correlation. Overall, plasma levels of D-dimer had a slight but significant correlation with most peak intensities in the total population. This result might be mainly determined by the correlation of the Non-AAD group, because the plasma levels of D-dimer in the Non-AAD group had a slight but significant correlation with most of the peak intensities, whereas the levels of D-dimer in the AAD group had almost no correlation with most of the peak intensities. Two high intensity Raman peaks at 1153 cm^{-1} and 1514 cm^{-1} in both groups were highly positive correlated (Non-AAD：Spearman r = 0.98, $p < 0.0001$; AAD：Spearman r = 0.96, $p < 0.0001$) . Essential amino acids at 750 cm^{-1} and 1004 cm^{-1} in both groups were moderately negative correlated (Non-AAD：Spearman r = -0.6, $p < 0.0001$; AAD：Spearman r = -0.35, $p < 0.0001$) . Similar correlatation were observed between 750 cm^{-1} and 1208 cm^{-1} (Non-AAD：Spearman r = -0.36, $p < 0.0001$; AAD：Spearman r = -0.46, $p < 0.0001$) while 1004 $cm^{-1}$and 1208 cm^{-1} in both groups were moderately positive correlated (Non-AAD：Spearman r = 0.22, $p < 0.0001$; AAD：Spearman r = 0.28, $p < 0.0001$) . The peaks at 842 cm^{-1} and 1448 cm^{-1}, corresponding to the CH2 bending mode of phospholipids, were highly positive correlated in both groups (Non-AAD：Spearman r = 0.71, $p < 0.0001$; AAD：Spearman r = 0.68, $p < 0.0001$) . The Raman peak at 1338 cm^{-1} (adenine and guanine) corresponding to DNA base pairs were highly negative correlated with the peaks of β carotene 1153 cm^{-1} (Non-AAD：Spearman r = -0.90, $p < 0.0001$; AAD：Spearman r = -0.84, $p < 0.0001$) and 1514 cm^{-1} (Non-AAD：Spearman r = -0.90, $p < 0.0001$; AAD：Spearman r = -0.83, $p < 0.0001$) .

3.4. Assessment of the discriminative performance and clinical usefulness

The candidated predictors, D-dimer, the Raman peak intensities at 505, 750, 842, 947, 1004, 1153, 1208, 1254, 1338, 1448, 1514, and 1655 cm^{-1}, were included in the original model, which were then reduced to eight potential predictors (D-dimer, the Raman peak intensities at 505, 750, 1153, 1208, 1254, 1448 and 1655 cm^{-1}) using LASSO regression analysis performed in the training cohort. The coefficients for these variables were shown in Table S1. In addition, a coefficient profile was depicted in Fig. 4A–and a cross-validated error plot of the LASSO regression model was displayed in Fig. 4B. The final selected model was the most regularized and parsimonious one that achieved a cross-validated error within one standard error of the minimum. It incorporated only eight variables.

As illustrated in Fig. 5A, the analysis of ROC curves for the aforementioned eight variables led to AUC values exceeding 0.5. Subsequent multivariate logistic analyses were conducted on various cohorts (data not presented). The AUCs of this model across diverse cohorts were depicted in Fig. 5B. Detailed results of ROC curve analyses can be found in Table 3. Combining peak intensities with D-dimer measurements yielded an AUC of 0.928 in the training cohort and an AUC of 0.936 in the internal test cohort, both significantly higher than those obtained from individual peak intensities or D-dimer alone. Furthermore, no significant differences were observed between sensitivity and specificity values within the training and internal test cohorts. Notably, when compared to using only D-dimer tests, combining different peak intensities with D-dimer exhibited relatively lower sensitivity but higher specificity levels. The final logistic model incorporated eight independent predictors and was transformed into a user-friendly nomogram. As demonstrated in the subsequent Fig. 6A, online dynamic nomogram accessible was displayed at https://nomofqjmxlh.shinyapps.io/dynnomapp/. The nomogram was established in the training cohort by incorporating the following eight parameters: D-dimer and

Table 2
The peak positions and tentative assignments of acquired Raman spectra.

Peak shift (cm^{-1})	Vibrational mode	Major assignments
505	S–S stretch mode	L-arginine
750	Ring vibration	L-tryptophan
842	CH2 bending mode	Phospholipids
947	C–C stretching vibration	α-Helix, proline, valine
1004	C–C symmetric stretch	Phenylalanine
1153	C–C stretch mode	β carotene
1208	Ring vibration	L-tryptophan
1254	C–N stretch mode	Amide-III
1338	CH3, CH2 wagging vibration	Adenine, guanine
1448	CH2 bending mode	Phospholipids
1514	C–C stretch mode	β carotene
1655	C–C stretching vibration	α-Helix, Collagen

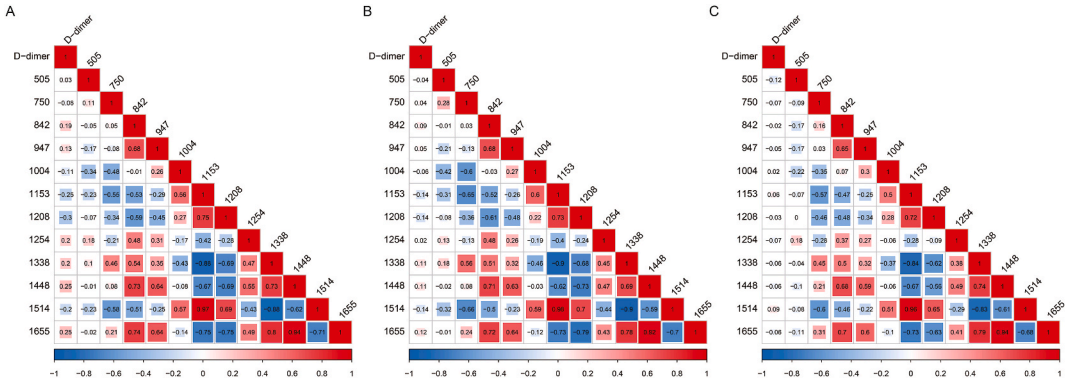

Fig. 3. Spearman correlation analysis was used to evaluate the correlation between D-dimer levels and candidated Raman peak intensities. (A) Serum samples of non-AAD and AAD groups. (B) Serum samples of non-AAD groups. (C) Serum samples of AAD groups.

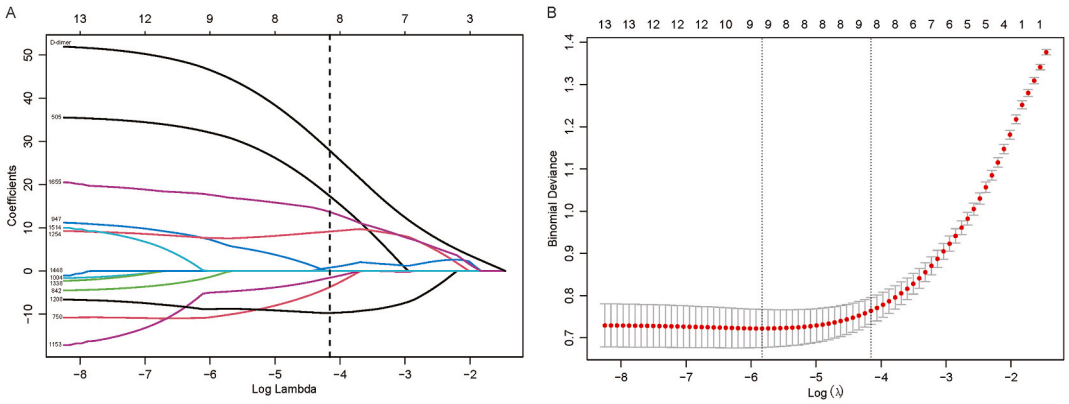

Fig. 4. A diagram illustrating the coefficient profile and cross-validated error of LASSO regression analysis performed on the training cohort was presented. (A) A coefficient profile of LASSO regression analysis was plotted. (B) A graph displaying the cross-validated error of the LASSO regression model was provided. LASSO = least absolute shrinkage and selection operator.

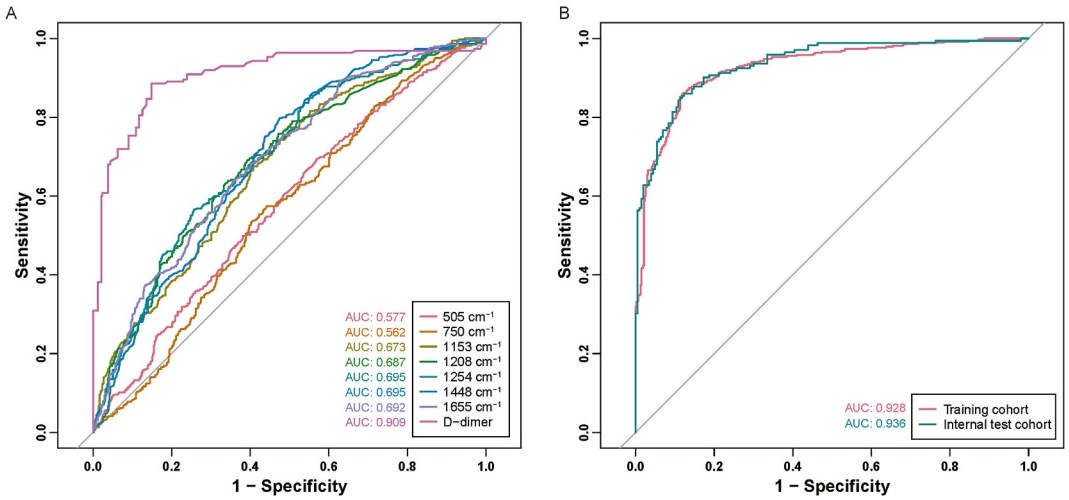

Fig. 5. ROC analysis was performed on candidated Raman peak intensities and D-dimer levels. (A) Individual ROC curves were generated for each potential predictor. (B) The combined ROC curves of the eight potential predictors were examined in both the training and internal test cohorts. ROC = receiver operating characteristic; AUC = area under the curve.

Table 3
Characteristics of ROC curves for training and internal test cohorts.

Variables	AUC (95 % CI)	Youden index	Cutpoint	Sensitivity	Specificity	Accuracy	PPV	NPV
Training	0.928(0.910–0.945)	0.741	0.400	86.2 %	87.9 %	87.1 %	85.1 %	88.8 %
Internal test	0.936(0.911–0.960)	0.737	0.403	86.0 %	87.7 %	86.9 %	85.5 %	88.1 %
D-dimer (1)	0.907(0.886–0.929)	0.732	0.013	88.4 %	84.8 %	86.4 %	82.5 %	90.0 %
D-dimer (2)	0.910(0.879–0.942)	0.733	0.011	89.7 %	83.7 %	86.4 %	82.1 %	90.6 %

Training indicates the training cohort of combined peak intensities with D-dimer measurements; Internal test indicates the internal test cohort of combined peak intensities with D-dimer measurements; D-dimer (1) indicates the training cohort of D-dimer measurement alone; D-dimer (2) indicates the internal test cohort of D-dimer measurement alone; AUC = area under the curve; CI = confidence interval; PPV = positive predictive value; NPV = negative predictive value.

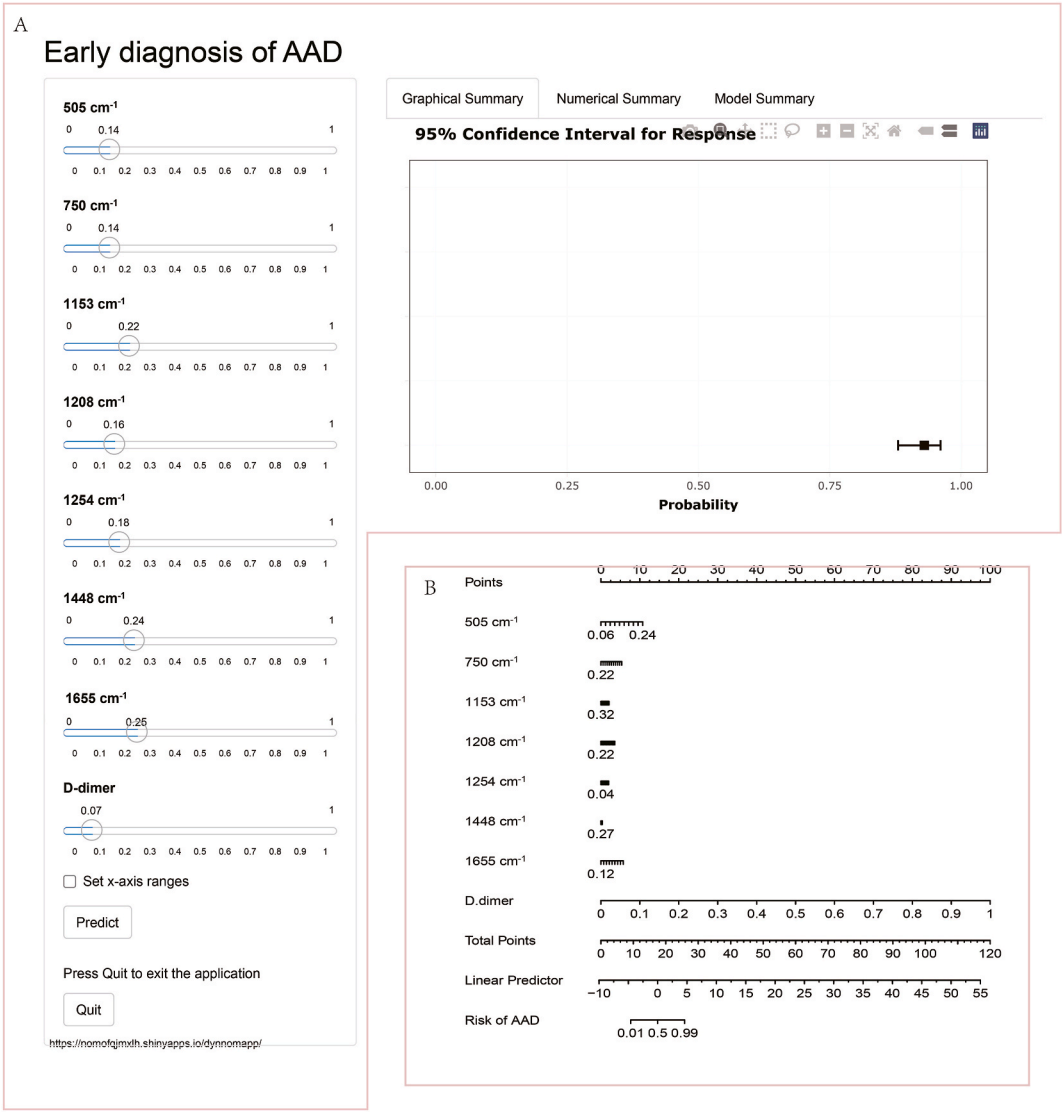

Fig. 6. Nomogram prediction model for early diagnosis of AAD. (A) Online dynamic nomogram accessible at https://nomofqjmxlh.shinyapps.io/dynnomapp/. (B) Established nomogram in the training cohort by incorporating the following eight parameters: D-dimer and the candidated Raman peak intensities at 505 cm^{-1}, 750 cm^{-1}, 1153 cm^{-1}, 1208 cm^{-1}, 1254 cm^{-1}, 1448 cm^{-1} and 1655 cm^{-1}.

the candidated Raman peak intensities at 505 cm^{-1}, 750 cm^{-1}, 1153 cm^{-1}, 1208 cm^{-1}, 1254 cm^{-1}, 1448 cm^{-1} and 1655 cm^{-1}(Fig. 6B).

The nomogram underwent rigorous internal validation and calibration via 1000 bootstrap analyses. Calibration plots (Fig. 7A and

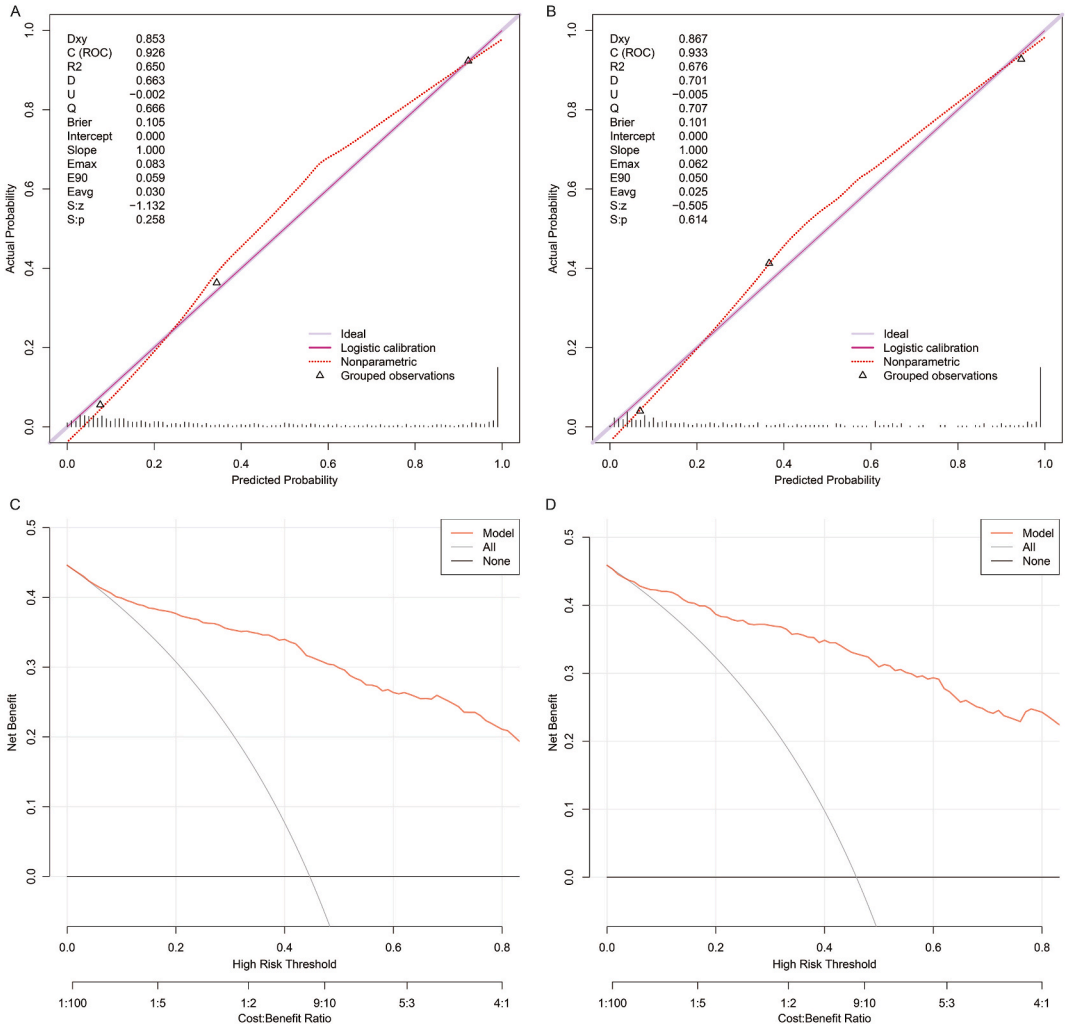

Fig. 7. The combination of eight potential predictors demonstrated its clinical utility through calibration plots and DCA curves. (A) Calibration plots for the nomogram were generated utilizing data from the training cohort. (B) Similarly, calibration plots for the nomogram were generated using data from the internal test cohort. (C) DCA was conducted on the training cohort to generate a DCA curve. (D) A DCA curve was generated using data from the internal test cohort. DCA = decision curve analysis.

B) demonstrated a robust correlation between observed and predicted groups across different cohorts, indicating the continued validity of the original nomogram for use in validation sets. The calibration curve closely resembled the ideal curve, suggesting consistent predicted results with actual findings. DCA curves (Fig. 7C and D) associated with the nomogram displayed net benefits at various threshold probabilities for diagnosing AAD. Utilizing these eight potential predictors to identify patients at risk of AAD outperformed both 'treat-none' and 'treat-all' approaches when encountering major flaws during diagnostic and decision-making processes. The DCA analysis revealed substantial net benefits for the clinical application of the nomogram. Moreover, NRI and IDI analyses in Table 4 indicated that combining these eight potential predictors significantly improved discrimination compared to a simple D-dimer test as a reference, with a continuous NRI of 39.8 % and an IDI of 9.95 % in the training cohort. This suggested that the combination of peak intensities and D-dimer, when compared to a simple D-dimer test alone, significantly enhanced correct classification by 39.8 % and overall predictive ability by 9.95 %. Similarly, in internal test cohorts, employing the D-dimer test as a benchmark, the integration of peak intensities and D-dimer achieved a 27.1 % improvement in correct classification and a 9.95 % enhancement in overall predictive capacity.

4. Discussion

In this study, the candidated peak intensities and D-dimer combination yielded positive net benefits and showed superior discrimination and calibration performance for AAD, exceeding the diagnostic capability of D-dimer alone. Consequently, the implementation of a combined approach that utilizing candidated peak intensities and D-dimer held promise as an efficient early

Table 4
NRI and IDI statistics for training and internal test cohorts.

Cohorts	Continuous NRI (95%CI, %)	*p* value [1]	IDI (95%CI, %)	*p* value [2]
Training	39.8(27.4–52.2)	0	9.95(7.83–12.1)	0
Internal test	27.1(8.54–45.7)	0.004	9.95(6.7–13.2)	0

NRI = net reclassification improvement; IDI = integrated discrimination improvement; CI = confidence interval.[1] *p* value of continuous NRI. [2]. *p* value of IDI.

diagnostic tool for AAD. To our knowledge, this study presented the first evaluation of the effectiveness of a diagnostic approach that combining Raman spectroscopy with D-dimer testing for identifying suspected AAD.

The main symptom of AAD is chest and back pain, which lacks specificity and is often similar to other sudden severe chest and back pain diseases, especially AMI and PE [3,4]. Although the first symptom of these acute and serious diseases is often the similar as chest and back pain, the treatment methods are completely different or even opposite. For example, when AAD is misdiagnosed as AMI, improper use of antiplatelet therapy may further increase the tear or even lead to aortic rupture. While early and accurate detection is critical to improving patient outcomes, there are substantial obstacles with the diagnostic techniques currently in use. Up to 30 %–40 % of patients remain undiagnosed prior to autopsy [22]. Imaging remains the primary method of diagnosis and differential diagnosis. Furthermore, as the gold standard for diagnosing AAD, aortic CTA also poses risks of radiation exposure, contrast agent allergies, and potential kidney damage. Transthoracic or transesophageal ultrasound, MRI and other image examination methods are time-consuming and laborious, and there are various risks in the examination process. Blood biomarker detection is more simple, rapid, economical and safe. Promising pathways for improving AAD early detection are presented by recent developments in serum biomarkers [23]. However, apart from D dimer, there are currently no other widely available AAD biomarkers with satisfactory sensitivity and specificity. The serum, which transports proteins, peptides, hormones, toxins, metabolites, nutrients, etc. throughout the body, reflects the biochemical changes occurring during the progression of various diseases. Consequently, serum samples, which obtained relatively easily, are optimally used for disease diagnosis. Raman spectroscopy has the capacity to provide changed spectral fingerprints in the vibrational frequencies of biomolecular bonding during the development of various diseases, thereby offering crucial information for disease diagnosis and prognosis. In this study, the spectra of the serum sample were recorded in the fingerprint area (400~1800 cm^{-1}) due to the presence of valuable diagnostic information. The reduction of β-carotene in the diseased serum samples aligned with previous research, including studies on cancer and inflammatory diseases [19,24,25]. Cell-free DNA, originating from cellular injury, served as an indicator of the degree of cell damage [9]. The intensities of Raman bands at 505 cm^{-1} (L-arginine), 947 cm^{-1} (α-Helix, proline, valine), 1254 cm^{-1} (Amide-III), and 1655 cm^{-1} (α-Helix, Collagen) in the serum of patients with AAD were higher. The increased intensities of these Raman peaks might be caused by worsening aortic lesions. This was consistent with the results of serum Raman spectroscopy studies of other cardiac diseases, where they also found increased intensities of some Raman peaks [9]. The increased concentration of cell-free DNA in the serum was proposed as a marker for AAD. Phospholipid peaks have been identified as diagnostic markers in previous studies [26]. The application of D-dimer as a promising biomarker for diagnosing suspected AAD was currently prevalent in clinical practice. Given the potential limitations of relying solely on D-dimer for diagnostic accuracy, it was advocated that the integration of multiple biomarkers could enhance diagnostic performance in clinical practice [5,27,28]. As such, we proposed the hypothesis that combining D-dimer detection with Raman spectroscopy could potentially augment the diagnostic precision of AAD.

In medical diagnosis, missed diagnosis and misdiagnosis are very serious events, so these indicators reflecting the positive and negative recognition effect are commonly used indicators. In this study, D-dimer measurements yielded an AUC of 0.907 in the training cohort (PPV 82.5 %, NPV90.0 %) and an AUC of 0.910 in the internal test cohort (PPV 82.1 %, NPV90.6 %). Due to the extremely high sensitivity and negative predictive value of D-dimer, its negativity has been used clinically as an important basis for excluding PE and deep venous thrombosis (DVT). Although the candidated Raman spectral peaks had some values in the identification of AAD, the superiorities were obviously worse than that of D-dimer. Given the tremendous destruction of AAD, minimal advances in its recognition are also extremely important for clinical outcomes. Therefore, the candidated different peak intensities and D-dimer combination model are used to distinguish the disease. When evaluating the improvement of predictive performance of the predictive model after incorporating Raman peak intensities with D-dimer, the new model improved the AUC but along with a slightly lower NPV.

DCA was frequently utilized to assess the clinical utility of markers or predictive models [29]. It aided in determining the most valuable and optimal choice for clinical application by identifying the model yielding the highest net benefit across all probability thresholds [30,31]. According to the DCA results, the combination of D-dimer and Raman spectroscopy led to an increase in net benefit and a reduction in false positive case. Furthermore, two new metrics, NRI and IDI, were adopted to give a comprehensive perspective on how much the predictive performance improves after the added value of a biomarker to an existing test [32,33]. In this study, the combination of D-dimer and the seven candidated Raman peak intensities significantly augmented discrimination power, as evidenced by a continuous NRI of 39.8 % and IDI of 9.95 % in the training cohort, as well as a continuous NRI of 27.1 % and IDI of 9.95 % in the internal test cohort. In practical clinical settings, the simultaneous measurements of D-dimer and Raman spectroscopy could provide clinicians with early and reliable screening outcomes for AAD. These results served as crucial references for further imaging decisions, accurately identifying patients who required emergency aortic imaging while optimizing diagnostic efficiency. The developed nomogram(Fig. 6) held several crucial clinical implications. Primarily, it supplied clinicians with a quantitative instrument for more precise prediction of AAD diagnosis, compared to relying solely on D-dimer levels, thereby enhancing risk stratification. Additionally, identifying high-risk individuals via this nomogram enabled timely interventions, which could potentially reduce mortality rates.

Especially in clinical practice, suspected AAD patients are often admitted from the emergency department. Raman spectroscopy combined with D-dimer indicators provides rapid diagnosis, enabling efficient triage of AAD.

In this study, we employed a large sample size to demonstrate the efficacy and practicality of combining D-dimer and Raman spectroscopy for diagnosis. Although this method offered advantages such as being risk-free, cost-effective, easy to measure, and suitable for clinical practice, there were areas that required further optimization and improvement in future studies. Firstly, it should be acknowledged that our findings were based on a single-center study, which inherently has limitations. Secondly, the complexity of the clinical setting exceeded that of the statistical model employed. Our logistic regression analysis only considered D-dimer levels and peak intensities, without incorporating other potentially influential parameters for better discrimination. It is possible that there may be unmeasured confounding factors not accounted for in our model. Thirdly, expanding the role of combining D-dimer and Raman spectroscopy in diagnosing acute aortic syndromes could benefit from including more patients with intramural hematoma and penetrating aortic ulcer alongside AAD cases. Additionally, although we explored various statistical indicators (NRI, IDI, and DCA) alongside ROC curves to evaluate the diagnostic performance and clinical utility of this combination approach, these findings remained exploratory at present. External validation across diverse populations at different institutions would be crucial in confirming the generalizability of our results.

5. Conclusions

In conclusion, the integration of D-dimer testing and Raman spectroscopy demonstrates significant potential for enhancing early differential diagnosis of AAD in clinical settings. Considering the escalating utilization of CT scans in emergency departments (e.g., a five-fold increase for chest pain and ten-fold increase for abdominal pain within a decade), this approach presents a prompt, cost-effective diagnostic technique that mitigates the exponential growth of emergency CT scans while reducing patient waiting time.

Funding

This study was partially supported by the National Natural Science Foundation of China (NSFC) (No. 82272247) and clinical research project of the first affiliated hospital of xi'an jiaotong university ([2021]20).

CRediT authorship contribution statement

Xuechang Han: Formal analysis, Data curation. **Shuang Wang:** Methodology, Formal analysis. **Runlu Cai:** Writing – review & editing, Supervision, Software. **Qiang Chen:** Formal analysis, Data curation. **Jing Li:** Investigation, Data curation. **Liang Zhong:** Investigation, Data curation. **Shuman Ji:** Investigation. **Xiaopeng Mei:** Supervision, Methodology. **Rongqian Wu:** Writing – review & editing, Methodology. **Yang Yan:** Writing – review & editing, Visualization, Supervision, Methodology. **Yi Lv:** Writing – review & editing, Visualization, Validation, Resources, Methodology. **Zhanqin Zhang:** Writing – review & editing, Writing – original draft, Supervision, Funding acquisition, Conceptualization.

Declaration of competing interest

The authors declare that they have no known competing financial interests or personal relationships that could have appeared to influence the work reported in this paper.

Acknowledgments

The authors thank Baoping Zhang of the Institute of Photonics and Photonic Technology at Northwestern University for her expert Raman testing of the serum samples.

Appendix A. Supplementary data

Supplementary data to this article can be found online at https://doi.org/10.1016/j.heliyon.2024.e32474.

References

[1] E.M. Isselbacher, O. Preventza, J. Hamilton Black, et al., 2022 ACC/AHA guideline for the diagnosis and management of aortic disease: a report of the American Heart association/American college of cardiology joint committee on clinical practice guidelines, Circulation 146 (24) (2022) e334–e482.
[2] T.T. Tsai, C.A. Nienaber, K.A. Eagle, Acute aortic syndromes, Circulation 112 (24) (2005) 3802–3813.
[3] S. Lovatt, C.W. Wong, K. Schwarz, et al., Misdiagnosis of aortic dissection: a systematic review of the literature, Am. J. Emerg. Med. 53 (2022) 16–22.
[4] J.R. McConaghy, M. Sharma, H. Patel, Acute chest pain in adults: outpatient evaluation, Am. Fam. Physician 102 (12) (2020) 721–727.
[5] E. Bossone, M. Czerny, S. Lerakis, et al., Imaging and biomarkers in acute aortic syndromes: diagnostic and prognostic implications, Curr. Probl. Cardiol. 46 (3) (2021) 100654.
[6] A.M. Ranasinghe, R.S. Bonser, Biomarkers in acute aortic dissection and other aortic syndromes, J. Am. Coll. Cardiol. 56 (19) (2010) 1535–1541.

[7] G. Cutshaw, S. Uthaman, N. Hassan, S. Kothadiya, X. Wen, R. Bardhan, The emerging role of Raman spectroscopy as an omics approach for metabolic profiling and biomarker detection toward precision medicine, Chem Rev. 123 (13) (2023) 8297–8346.
[8] A. Chaichi, A. Prasad, M.R. Gartia, Raman spectroscopy and microscopy applications in cardiovascular diseases: from molecules to organs, Biosensors 8 (4) (2018).
[9] R.V. John, T. Devasia, M. N, J. Lukose, S. Chidangil, Micro-Raman spectroscopy study of blood samples from myocardial infarction patients, Lasers Med Sci 37 (9) (2022) 3451–3460.
[10] Q. Chen, T. Shi, D. Du, et al., Non-destructive diagnostic testing of cardiac myxoma by serum confocal Raman microspectroscopy combined with multivariate analysis, Anal. Methods 15 (21) (2023) 2578–2587.
[11] Y. Ren, Q. Tang, W. Liu, Y. Tang, R. Zhu, B. Li, Serum biomarker identification by mass spectrometry in acute aortic dissection, Cell. Physiol. Biochem. 44 (6) (2017) 2147–2157.
[12] H. Wu, P. Ding, J. Wu, et al., A new online dynamic nomogram: construction and validation of a predictive model for distant metastasis risk and prognosis in patients with gastrointestinal stromal tumors, J. Gastrointest. Surg. 27 (7) (2023) 1429–1444.
[13] R. Erbel, V. Aboyans, C. Boileau, et al., ESC Guidelines on the diagnosis and treatment of aortic diseases: document covering acute and chronic aortic diseases of the thoracic and abdominal aorta of the adult. The Task Force for the Diagnosis and Treatment of Aortic Diseases of the European Society of Cardiology (ESC), Eur. Heart J. 35 (41) (2014) 2873–2926.
[14] F. Giachino, M. Loiacono, M. Lucchiari, et al., Rule out of acute aortic dissection with plasma matrix metalloproteinase 8 in the emergency department, Crit. Care 17 (1) (2013) R33.
[15] K.A. Marill, Serum D-dimer is a sensitive test for the detection of acute aortic dissection: a pooled meta-analysis, J. Emerg. Med. 34 (4) (2008) 367–376.
[16] A. Shimony, K.B. Filion, S. Mottillo, T. Dourian, M.J. Eisenberg, Meta-analysis of usefulness of d-dimer to diagnose acute aortic dissection, Am. J. Cardiol. 107 (8) (2011) 1227–1234.
[17] L. Lu, L. Shi, J. Secor, R. Alfano, Resonance Raman scattering of beta-carotene solution excited by visible laser beams into second singlet state, J. Photochem. Photobiol., B 179 (2018) 18–22.
[18] X. Wang, F. Xie, Y. Yang, J. Zhao, G. Wu, S. Wang, Rapid diagnosis of ductal carcinoma in situ and breast cancer based on Raman spectroscopy of serum combined with convolutional neural network, Bioengineering (Basel). 10 (1) (2023).
[19] M. Bahreini, A. Hosseinzadegan, A. Rashidi, S.R. Miri, H.R. Mirzaei, P. Hajian, A Raman-based serum constituents' analysis for gastric cancer diagnosis: in vitro study, Talanta 204 (2019) 826–832.
[20] S. Zhu, Y. Li, H. Gao, et al., Identification and assessment of pulmonary Cryptococcus neoformans infection by blood serum surface-enhanced Raman spectroscopy, Spectrochim. Acta Mol. Biomol. Spectrosc. 260 (2021) 119978.
[21] G. Lu, X. Zheng, X. Lu, P. Chen, G. Wu, H. Wen, Label-free detection of echinococcosis and liver cirrhosis based on serum Raman spectroscopy combined with multivariate analysis, Photodiagnosis Photodyn. Ther. 33 (2021) 102164.
[22] T. Deng, Y. Liu, A. Gael, et al., Study on proteomics-based aortic dissection molecular markers using iTRAQ combined with label free techniques, Front. Physiol. 13 (2022) 862732.
[23] H. Chen, Y. Li, Z. Li, Y. Shi, H. Zhu, Diagnostic biomarkers and aortic dissection: a systematic review and meta-analysis, BMC Cardiovasc. Disord. 23 (1) (2023) 497.
[24] C. Rosa, C. Franca, Vieira S. Lanes, et al., Reduction of serum concentrations and synergy between retinol, beta-carotene, and zinc according to cancer staging and different treatment modalities prior to radiation therapy in women with breast cancer, Nutrients 11 (12) (2019).
[25] L. Wang, C. Ding, F. Zeng, H. Zhu, Low levels of serum beta-carotene and beta-carotene/retinol ratio are associated with histological severity in nonalcoholic fatty liver disease patients, Ann. Nutr. Metab. 74 (2) (2019) 156–164.
[26] C. Li, S. Liu, Q. Zhang, et al., Combining Raman spectroscopy and machine learning to assist early diagnosis of gastric cancer, Spectrochim. Acta Mol. Biomol. Spectrosc. 287 (Pt 1) (2023) 122049.
[27] A. Forrer, F. Schoenrath, M. Torzewski, et al., Novel blood biomarkers for a diagnostic workup of acute aortic dissection, Diagnostics 11 (4) (2021).
[28] M. Zhang, Z.D. Hu, Suggestions for designing studies investigating diagnostic accuracy of biomarkers, Ann. Transl. Med. 7 (23) (2019) 788.
[29] B. Van Calster, L. Wynants, J.F.M. Verbeek, et al., Reporting and interpreting decision curve analysis: a guide for investigators, Eur. Urol. 74 (6) (2018) 796–804.
[30] I. Hozo, A. Tsalatsanis, B. Djulbegovic, Monte Carlo decision curve analysis using aggregate data, Eur. J. Clin. Invest. 47 (2) (2017) 176–183.
[31] E.R. Dadashzadeh, P. Bou-Samra, L.V. Huckaby, et al., Leveraging decision curve analysis to improve clinical application of surgical risk calculators, J. Surg. Res. 261 (2021) 58–66.
[32] M.J. Pencina, R.B. D'Agostino, R.B. D'Agostino Jr., R.S. Vasan, Evaluating the added predictive ability of a new marker: from area under the ROC curve to reclassification and beyond, Stat. Med. 27 (2) (2008) 157–172. ; discussion 207-112.
[33] N.R. Cook, O.V. Demler, N.P. Paynter, Clinical risk reclassification at 10 years, Stat. Med. 36 (28) (2017) 4498–4502.